Deciphering fermionic matter: from holography to field theory

Meszéna, B.

Chapter 3

Non-perturbative emergence of non-Fermi liquid behaviour in $d = 2$ quantum critical metals

3.1 Introduction

A complete classification of infrared universality classes for phases of quantum matter at finite density is an open problem in condensed matter theory. Experimentally, a number of fermionic states of matter that exhibit breakdown of the quasiparticle Fermi-liquid paradigm [7] are known to exist, e.g. the strange metallic phase of unconventional superconductors [8] or the non-Fermi liquid phase of graphene [9, 10]. Theoretically, however, they are not understood. These phases are strongly interacting and this prevents the use of most conventional approaches that rely on perturbation theory.

One important scenario which is widely believed to cause the partial destruction of Fermi surfaces and substantial change of transport properties of the electronic state in high-T_c compounds [11], heavy fermion systems [12], and Mott insulators [13, 14] is the interaction of electronic quasiparticles with gapless bosons. The underlying physics is the proximity of a quantum critical point and these bosons are the protected emergent gapless collective degrees of freedom [15, 5, 11]. The nature of the fermion-boson interaction is determined by the precise details of the quantum critical point — ferromagnetic [17] or antiferromagnetic [18] spin density waves, Kondo impurities [19], etc; see [6] for a review.

Qualitatively the simplest model that should already capture the nontrivial physics is the theory of spinless fermions at finite density interacting with a massless scalar through a straightforward Yukawa coupling. The

action of this theory is:

$$S = \int \mathrm{d}x\mathrm{d}y\mathrm{d}\tau \left[\psi^\dagger \left(-\partial_\tau + \frac{\nabla^2}{2m} + \mu \right) \psi + \frac{1}{2} \left(\partial_\tau \phi \right)^2 + \frac{1}{2} \left(\nabla \phi \right)^2 + \lambda \phi \psi^\dagger \psi \right]. \tag{3.1}$$

This model is believed to describe the Ising-nematic transition (see e.g. [11, 20]), observed for example in $YBa_2Cu_3O_y$, There, the meaning of the boson is the fluctuating order parameter related to the $C_4 \to C_2$ symmetry breaking of the electronic correlations. In the ordered phase the mass square of the boson is positive $M^2 > 0$, while in the disordered phase $M^2 < 0$. For non-zero mass we obtain a regular Fermi-liquid at low frequency. By choosing $M = 0$ we tune our theory to criticality where we expect non-Fermi liquid behavior. The model is also closely related to the theory of fermionic spinon excitations in a spin density wave minimally coupled to $U(1)$; at low energies only the transverse component of the gauge field survives and acts as the scalar above (see e.g. [24]).

Eq. (3.1) and related models of finite density fermions coupled to critical bosons were first studied in detail by Hertz [15] and Millis [5], but their results do not apply in 2+1 dimensions. For $d = 2$ the coupling λ is relevant [11], and can drive the system to a qualitatively new groundstate. This novel non-Fermi liquid groundstate is out of range of perturbation theory, and the fermion sign problem prevents us from using efficient numerical techniques.

Our work continues on a recent revival of interest in determining this groundstate. The crucial physics that is thought to control the non-Fermi liquid behavior is the Landau damping: the quantum fermion-loop corrections to the boson two-point correlation function/self-energy. By extending the model to an arbitrary number of fermions N_f and bosons N_b, one can enhance this physics in a limit where the number of fermion flavors N_f is much larger than the number of bosonic degrees of freedom ($N_f \gg N_b$); it is easily seen at the one loop level that this enhances the "Landau-damping" diagram in Fig. 3.1(b) compared to the self-energy Fig. 3.1(a). In this $N_f \gg N_b$ regime the problem of a Fermi surface coupled to the Ising nematic and spin density wave order parameters has been considered in [20, 21] and an extensive perturbative renormalization group analysis has been performed up to three loops (higher order effects are investigated in [22, 23]). However, as pointed out in these papers and [24], in the (vector) large N_f expansion one still needs to sum infinitely many diagrams.

Figure 3.1. One loop corrections to fermion (a) and boson (b) self-energies due to Yukawa interaction. For a gapless boson (b) is the one loop contribution to Landau damping: this contribution to the self-energy can dominate in the IR. This term (b) is clearly proportional to the number of fermions N_f in contrast to the one-loop correction to the fermion self-energy (a). In the limit $N_f \gg N_b$ the boson self-energy/Landau damping therefore dominates, whereas it is suppressed in the opposite limit $N_f \ll N_b$.

(A well-defined expansion can be obtained by introducing an arbitrary dynamical critical exponent for the boson, z_b, as an extra control parameter [25].)

Here, however, we show that Landau damping is not essential to obtain exotic non-Fermi liquid physics in the IR. We will study correlation functions of the theory in the opposite limit $N_f \to 0$; $N_b = 1$. This so-called quenched limit discards all fermion loop contributions. As $N_f \ll N_b$ it shares common ground with recent matrix large N expansions of this model where the boson is taken to transform in the adjoint of an $SU(N)$ and the fermions in the fundamental, see e.g. the studies [26–29], but the strict quenched limit is more comprehensive. In the matrix large N limit where $N_f = N$ and $N_b = N^2$ with $N \gg 1$, not only the diagrams with fermion loops but also diagrams with crossed boson lines are suppressed (Fig. 3.2), whereas these are kept in the quenched approximation. By inspection of the associated momentum integral it is clear, however, that crossed boson corrections are important contributions to the IR physics. The IR of the quenched theory will therefore be different from the large N matrix limit and perhaps closer to that of the full theory.

Physically the quenched approximation we study here means the following: as pointed out in [29] there is a distinct energy scale where Landau damping becomes important. This is the scale where the fermion one-loop correction proportional to N_f becomes comparable to the leading boson dispersion — this happens at $E_{\rm LD} \sim \sqrt{\lambda^2 N_f k_F}$ (see the end of section 3.2.1). By considering small N_f we are suppressing this scale and we are zooming in on the energy regime directly above the Landau damping scale

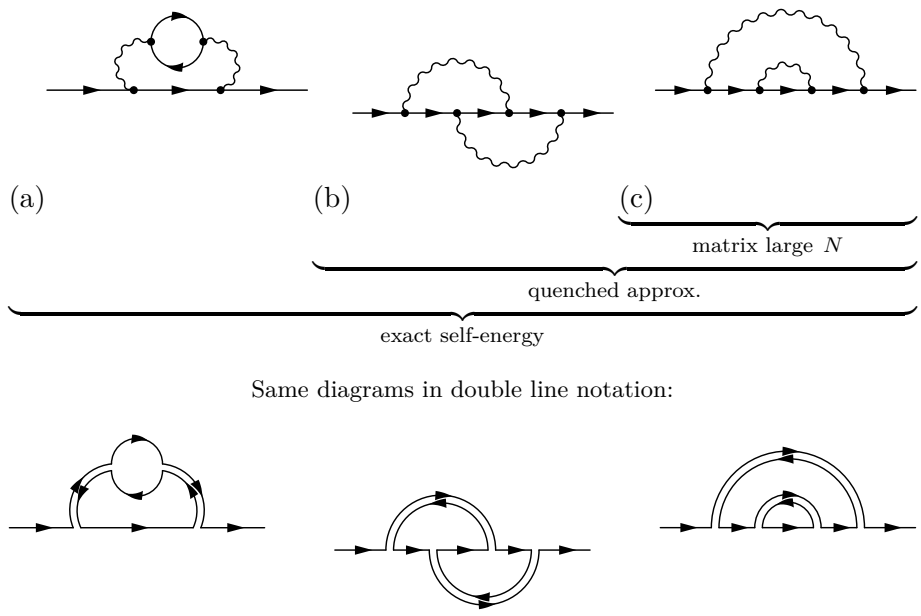

Figure 3.2. The two-loop contributions to the fermion self-energy in theory in Eq. (4.2). The quenched limit where $N_f \to 0$ only suppresses the fermion loop contribution Fig. (a), whereas matrix large N limits, where the boson is a $N \times N$ matrix $\phi_i{}^j$ and the fermion a N-component vector ψ_i also suppress crossed diagrams of type (b). This is evident in double line notation of the same Feynman diagrams where the fermion is written as a single line (it has one index) and the matrix-valued boson as two lines (it has two indices). Indices have to match at interactions; each closed loop therefore corresponds to a sum over this index and gives a weight N to the diagram. We then see that the crossed diagram has no loops and is thus sub-dominant in N to other diagrams at the same order in the coupling constant.

E_{LD} (see Fig. 3.3).[1]

The quenched approximation has an additional benefit. Under the assumption that that the cut-off of the boson is much smaller than the Fermi momentum ($k_F \gg \Lambda_{\mathrm{UV}}$), the small N_f limit also allows us to consistently focus on a small local patch (see Fig. 3.3) around the Fermi surface where the fermionic excitations disperse linearly. The reason the curvature effects are negligible and the global structure of the Fermi surface becomes irrelevant, is that their influence on the IR physics is also through Landau damping. If the Landau damping is not negligible, one does have to either work with the full Fermi surface (i.e. in [26–29] for the case of spherical Fermi surface) or at least consider the antipodal patch since the dominant contribution is coming from there [20, 21]. Specifically, as we discuss below, Landau damping depends both on the Fermi-surface curvature $\kappa \sim \frac{1}{k_F}$ and N_f as N_f/κ. After the quenched approximation $N_f \to 0$ for fixed κ, we may subsequently take κ small as well.

The remarkable fact is that with these approximations the fermion Green's function can be determined exactly (directly in $d = 2$ spatial dimensions). We achieve this by solving the differential equation for the Green's function in a background scalar field and then evaluating the bosonic path integral. Similar functional techniques have been used in high energy physics, for example in the study of high temperature QED plasma [30], lattice QCD [31] or for solving the so-called Bloch-Nordsieck model (which is QED in the quenched approximation) [32–34, 31, 35]. In condensed matter context, the fact that the fermion spectral function is exactly solvable in these limits was also observed for finite density fermions coupled to a transverse gauge field by Khveshchenko and Stamp [36] and independently by Ioffe, Lidsky, Altshuler and Millis [37, 38], though the latter solve the model by bosonization.

At the technical level, the reason the spectral function can be solved exactly in the quenched limit is that propagators of linearly dispersing fermions (the local patch approximation) obey special identities. These allow a rewriting of the loop expansion in such a way that it can be resummed completely, or rather that it can be recast as the solution to a tractable differential equation. We show this in section 3.2. Note, that our method does not rely on renormalization group techniques. When we are to define an RG flow, we have to choose a proper decimation scheme.

[1] There are other ways to suppress the Landau damping physics, e.g. by considering large (UV) Fermi velocity, but we will not be considering these cases here.

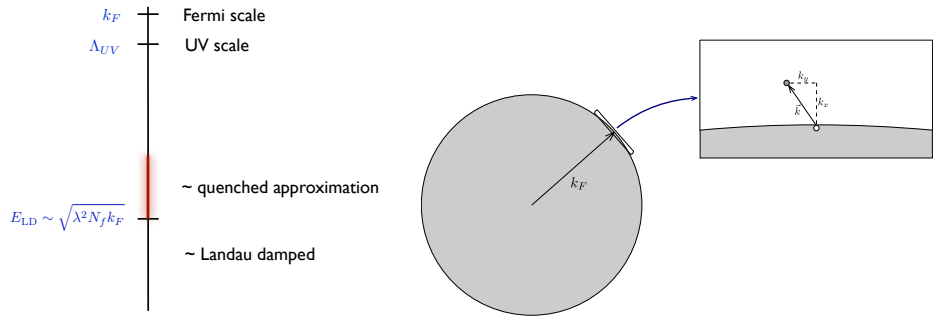

Figure 3.3. Left: The energy scales relevant to 2+1 dim. finite density fermions coupled to a massless boson. We assume the theory is already truncated at a UV cut-off $\Lambda_{\rm UV}$ lower than the Fermi scale k_F. The quenched $N_f \to 0$ limit focuses in on the intermediate energy regime right above the scale $E_{\rm LD} \sim \sqrt{\lambda^2 N_f k_F}$ where Landau damping becomes important.
Right: A small patch of the Fermi surface. In a small region near the Fermi level the surface curvature is negligible. Fermionic excitations can acquire both orthogonal k_x and tangent k_y momenta, but the latter does not contribute to the kinetic energy of the excitation. In the $N_f \to 0$ limit each patch decouples from other parts of the Fermi surface.

In relativistic field theories, it is natural to define the cut-off in a way that maintains the Lorentz invariance, while for the non-relativistic model of critical metals the choice of the cut-off is ambiguous, see e.g. [26].

These exact results in quenched approximation then allow us to establish that the IR fermion physics, even in the absence of Landau damping, is already that of a non-Fermi liquid. Specifically we show in section 3.3 that:

- The naive free Fermi surface breaks apart into three. A thin external shell of it splits apart from the rest, and we effectively have three nested singular surfaces (see Fig. 3.4). This immediately follows from the fact that in a region around the original (free) Fermi level the dispersion of fermion changes sign, $\frac{d\omega}{dk_x} < 0$. This can be interpreted as a topological instability of the Fermi surface [22], as the dispersion curve must cross the Fermi energy two more times

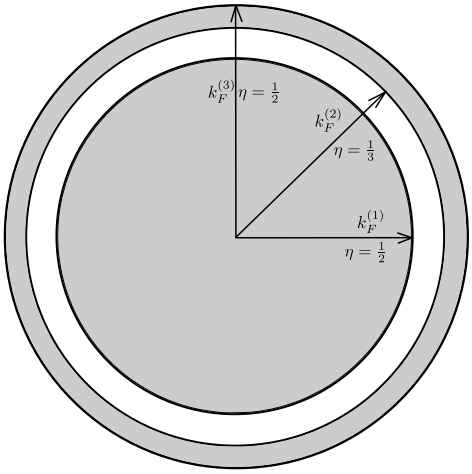

Figure 3.4. The emergent Fermi surface structure at low energy in the 2+1 dimensional quenched planar patch quantum critical metal. Due to the interactions the naive single Fermi surface is topologically unstable. The excitations around the Fermi surfaces are not well-defined quasiparticles, instead they have a continuous spectrum corresponding to a Green's function of the type $G(\omega, k) \sim (\omega - vk)^{-\eta}$ with scaling dimensions η. The different values of η at each of the emergent singular surfaces are mentioned.

to connect to the free UV theory. Luttinger's theorem nevertheless continues to hold.

- The Fermi-liquid quasiparticle pole is destroyed by the interaction with the critical boson. Instead the spectrum is singular everywhere on the dispersion curve. Specifically near the three Fermi surfaces the singular Green's function takes a scaling form with different scaling dimensions. Around the original Fermi momentum the Green's function behaves as $G(\omega, k_x) \sim (\omega + ck_x)^{-1/3}$, where c is the dispersion velocity of the boson; around the two split-off Fermi surfaces behaves as $G(\omega, k) \sim (\omega - v^* k_x)^{-1/2}$ with v^* an emergent dispersion velocity $0 < v^* < v_F$.

We conclude this chapter with a brief outlook in section 4.6.

3.2 2+1 dimensional quantum critical metals in the patch approximation

As stated, the theory we study is that of N_f spinless fermionic flavours at finite density minimally coupled to a critical (relativistically dispersing) boson in $2+1$ dimensions. It has the Euclideanized action

$$S = \int \mathrm{d}x\mathrm{d}y\mathrm{d}\tau \left[\psi_j^\dagger \left(-\partial_\tau + \frac{\nabla^2}{2m} + \mu\right)\psi^j + \frac{1}{2}\left(\partial_\tau\phi\right)^2 + \frac{1}{2}\left(\nabla\phi\right)^2 + \lambda\phi\psi_j^\dagger\psi^j\right] \tag{3.2}$$

with $j = 1 \ldots N_f$; we will show below that the rotation back to real time has no ambiguities. Assuming that the theory is still weakly coupled at scales much below the Fermi momentum k_F, we may make a local approximation around a patch of the Fermi surface and truncate the fermion kinetic term to (Fig. 3.3) [11]

$$S_P = \int \mathrm{d}x\mathrm{d}y\mathrm{d}\tau \left[\psi_j^\dagger(-\partial_\tau + iv\partial_x)\psi^j + \right. \tag{3.3}$$

$$\left. + \frac{1}{2}\left(\partial_\tau\phi\right)^2 + \frac{1}{2}\left(\partial_x\phi\right)^2 + \frac{1}{2}\left(\partial_y\phi\right)^2 + \lambda\phi\psi_j^\dagger\psi^j\right]. \tag{3.4}$$

Two comments are in order. (1) Though it is very well known that the leading "Fermi surface curvature" correction to the kinetic term $\mathcal{L}_{\mathrm{curv}} = -\kappa\psi_j^\dagger\partial_y^2\psi^j/2 + \ldots$ is a dangerously irrelevant operator important for fermion loops even at low energies, in the $N_f \to 0$ limit (where there are no fermion loops) this operator is safely irrelevant and can be consistently neglected for physics below the scale set by $1/\kappa$. We will show here through exact results that the minimal theory in Eq. (4.2) already has a very non-trivial IR. We shall comment on the relevance of $\mathcal{L}_{\mathrm{curv}}$ to our results below. (2) From a Wilsonian point of view, self-interactions of the boson should also be included. We leave the effect of this term for future investigations and take the action S_P as given from here on and study it on its own.[2]

[2]Note that, although the kinetic term is effectively $(1+1)$-dimensional, the properties of fermionic field are still strongly dependent on the dimensionality of the system, because the fermions interact with the $(d+1)$-dimensional boson. An instructive way to think about the fermion dynamics in dimensions parallel to the Fermi surface, is to Fourier transform in those directions. Because the kinetic term does not depend on these directions, the parallel momenta act as additional global quantum numbers. E.g. in $d = 2$, one therefore has an infinite set of one-dimensional fermionic subsystems, labeled by k_y. The Yukawa interaction with the bosons then describes the interactions between these many one-dimensional subsystems.

Throughout this chapter we are mostly interested in the case where the characteristic speed $c = 1$ of the critical bosonic excitations is larger than the Fermi velocity, $c > v$. This need not be the case in the UV. However, as was recently argued [27, 29], the Fermi velocity decreases substantially under the RG flow and because in our analysis we consider energies below a cut-off $\Lambda_{\mathrm{UV}} \ll k_{\mathrm{f}}$, we take this condition for granted as a starting point.

In $d = 2$ spatial dimensions the Yukawa coupling is relevant — λ has scaling dimension $1/2$ — and the theory will flow to a new IR fixed point. Rather than focusing on a complete understanding of the IR of the action Eq. (4.2), we will focus only on understanding a single correlation function: the fermion spectral function. Coupling the fermionic fields to external sources

$$Z[J, J^\dagger] = \int \mathcal{D}\psi^j \mathcal{D}\psi_j^\dagger \mathcal{D}\phi \exp\left(-S_P - J_j^\dagger \psi^j - \psi_j^\dagger J^j\right), \tag{3.5}$$

the fermionic integral is Gaussian and can be easily evaluated yielding

$$Z[J] = \int \mathcal{D}\phi \, \exp\left(-S_b[\phi] - S_{\mathrm{det}}[\phi] - \int d^3z d^3z' J_i^\dagger(z) G_j^i[\phi](z;z') J^j(z')\right), \tag{3.6}$$

with

$$\begin{aligned} S_b &= \int \mathrm{d}x\mathrm{d}y\mathrm{d}\tau \left[\frac{1}{2}\left(\partial_\tau \phi\right)^2 + \frac{1}{2}\left(\partial_x \phi\right)^2 + \frac{1}{2}\left(\partial_y \phi\right)^2\right] \\ S_{\mathrm{det}} &= \int \mathrm{d}x\mathrm{d}y\mathrm{d}\tau \left[-N_f \mathrm{Tr} \ln G^{-1}[\phi]\right] \end{aligned} \tag{3.7}$$

and $G^i{}_j[\phi](z;z') = \delta_j^i G[\phi](\tau, x, y; \tau', x', y')$ is the fermionic propagator in presence of a background bosonic field configuration. By definition it satisfies

$$\begin{aligned} \left(-\partial_\tau + iv\partial_x + \lambda\phi(\tau, x, y)\right) G[\phi](\tau, x, y; \tau', x', y') = \\ = \delta(\tau - \tau')\delta(x - x')\delta(y - y') \end{aligned} \tag{3.8}$$

Taking functional derivatives with respect to the sources, the full fermion Green's function is then given by a path integral over only the bosonic field:

$$\langle \psi_j^\dagger(z)\psi^i(0)\rangle_{\mathrm{exact}} = \delta_j^i G(z, z') = \delta_j^i \frac{\int \mathcal{D}\phi \, G[\phi](z, z') e^{-S_b[\phi] - S_{\mathrm{det}}[\phi]}}{\int \mathcal{D}\phi \, e^{-S_b[\phi] - S_{\mathrm{det}}[\phi]}}. \tag{3.9}$$

3.2.1 The $N_f = 0$ quenched approximation and Landau damping

We will evaluate this integral in the quenched or Bloch-Nordsieck approximation. This is a well known ad hoc approximation in lattice gauge theory [31] and finite temperature QED [32–35] whereby all contributions from S_{det} are ignored: one sets the one-loop (fermion) determinant to one by hand. In our context we can make this approximation precise. Eq. (3.7) shows that S_{det} is directly proportional to N_f, whereas no other terms are. From Eq. (3.9) it is then clear that this approximation computes the leading contribution to the full fermion Green's function in the limit $N_f \to 0$. Note that we consider the N_f limit within correlation functions and not directly in the partition function.

Diagrammatically this means that one considers only contributions to the full Green's functions that do not contain fermion loops. Fermion loop corrections to the bosonic propagator, however, encode the physics of Landau damping. As discussed, this is important in the deep infrared and requires treatment of the dangerously irrelevant quadratic corrections to the kinetic term $\mathcal{L}_{\text{curv}}$ due to Fermi surface curvature. It is its Landau damping contribution that redirects the RG flow. This can be seen from the one-loop "polarization" correction Π to the boson-propagator at finite N_f.

$$G_B^{-1} = G_{B0}^{-1} + \Pi = q_0^2 - q_x^2 - q_y^2 + \Pi \tag{3.10}$$

The form of the polarization depends on the concrete form of the Fermi surface. In case of a spherical Fermi surface with Fermi momentum k_F its form at the one-loop level for large k_F equals

$$\Pi_{1S}\left(q_0, q_x, q_y\right) = \frac{\left(2\pi\right)^2 \lambda^2 k_F N_f}{v} \left(\frac{|q_0|}{\sqrt{q_0^2 + v^2(q_x^2 + q_y^2)}} \right). \tag{3.11}$$

The Fermi surface curvature κ is inversely proportional to the Fermi momentum $\kappa \sim 1/k_F$, therefore the polarization is controlled by the combination N_f/κ. One immediately sees that there is an energy scale $E_{\text{LD}} \sim \sqrt{\lambda^2 N_f/\kappa}$ where the polarization becomes of order of the leading boson dispersion, where perturbation theory must break down and the theory changes qualitatively.[3] On the other hand, as we explained in the introduction, above this scale E_{LD} one ought to be able to neglect

[3] One may worry that at higher loop order a different scale arises. It turns out,

these contributions to the boson propagator [29, 39]. This is therefore the regime captured by the $N_f \to 0$ limit. Since this $N_f \to 0$ limit tames the dangerous nature of irrelevant Fermi surface curvature κ, this also justifies the patch approximation and linearization of the fermion dispersion relation. In this chapter we focus on this regime; we leave the effects of Landau damping captured by the $\mathcal{O}(N_f)$ corrections for Chapter 4.

The remarkable fact is that in this regime $G_{\text{full}}(z; z')$ can be determined exactly, as we will now show. This is because the fermion two-point function in the presence of a background field $G[\phi](z; z')$ depends on the background bosonic field exponentially. The overall path integral over ϕ therefore remains Gaussian even in presence of the Yukawa interaction. This gives us qualitatively new insight in the physics right above E_{LD}.

3.2.2 The exact fermion Green's function

First, we determine the fermion Green's function in the presence of an external boson field $G[\phi]$. Rather then working in momentum space, it will be much more convenient to work in position space. Note that because the background scalar field $\phi(\tau, x, y)$ can be arbitrary, the fermionic Green's function $G[\phi]$ is not translationally symmetric. However, translational invariance will be restored after evaluating the path integral over ϕ.

Rewriting the background dependent Green's function as

$$G[\phi](\tau_1, x_1, y_1; \tau_2, x_2, y_2) = \tilde{G}_0(\tau_1 - \tau_2, x_1 - x_2, y_1 - y_2) \exp\left(-\lambda V[\phi](\tau_1, x_1, y_1; \tau_2, x_2, y_2)\right), \tag{3.12}$$

with $\tilde{G}_0$ the translationally invariant free Green's function in real space

$$\tilde{G}_0(\tau, x, y) = -\frac{i}{2\pi} \frac{\text{sgn}(v)}{x + iv\tau} \delta(y) \equiv G_0(\tau, x)\delta(y), \tag{3.13}$$

it is readily seen that the solution to the defining Eq. (3.8) is given by

$$V[\phi](\tau_1, x_1, y_1; \tau_2, x_2, y_2) = \int \mathrm{d}x\mathrm{d}y\mathrm{d}\tau \left[\tilde{G}_0(\tau_1 - \tau, x_1 - x, y_1 - y) - \tilde{G}_0(\tau_2 - \tau, x_2 - x, y_2 - y)\right] \phi(\tau, x, y), \tag{3.14}$$

however, that at higher order, contributions to Π are subleading in k_F compared to the one-loop result. This is because for linearized fermion dispersion ($\kappa \to 0$) the properly symmetrized closed fermion loops with more than two fermion lines vanishes [54]. In this chapter where we take the $N_f/\kappa \to 0$ limit we therefore use the unmodified boson propagator G_{B0}.

To be more precise, we need to ensure that the background dependent Green's function (3.12) satisfies proper boundary conditions as well. We did so by considering the problem at finite temperature and volume and taking explicitly the continuum limit. The compact analog of (3.12) has to satisfy antiperiodic boundary condition along the imaginary time direction and periodic boundary condition along the spatial direction. This can be achieved by taking the periodic free fermion Green's function ($\tilde{G}_0^P$) in the exponent Eq. 3.14 and the antiperiodic one ($\tilde{G}_0^{AP}$) in Eq. 3.12. In the continuum limit, however, their functional forms are indistinguishable, and we denote them with the same symbol ($\tilde{G}_0$).

The insight is that the only dependence on ϕ in the background dependent Green's function is in the exponential factor $V[\phi]$ and that this dependence is linear. In combination with the quenched $N_f \to 0$ limit, the path-integral over ϕ Eq. (3.9) needed to obtain the full Green's function is therefore Gaussian, and we can straightforwardly evaluate this to (3.9) to obtain

$$G\left(\tau_1, x_1, y_1; 0\right) = G_0\left(\tau_1, x_1\right) \delta(y_1) \exp\left[I(\tau_1, x_1; 0)\right] \tag{3.15}$$

with

$$I(\tau_1, x_1; 0) = \frac{\lambda^2}{2} \int \mathrm{d}x \mathrm{d}\tau \mathrm{d}x' \mathrm{d}\tau' M(\tau_1 - \tau, x_1 - x; -\tau, -x) \cdot \tag{3.16}$$

$$\cdot G_B(\tau - \tau', x - x', 0) M(\tau_1 - \tau', x_1 - x'; -\tau, -x), \tag{3.17}$$

where

$$M(\tau_1, x_1; \tau_2, x_2) = G_0(\tau_1, x_1) - G_0(\tau_2, x_2) \ , \tag{3.18}$$

and $G_B(\tau - \tau', x - x', y - y') = G_B(\tau, x, y; \tau', x', y')$ equal to the translationally invariant free boson propagator defined by

$$\left(\partial_\tau^2 + \nabla^2\right) G_B(\tau, x, y; \tau', x', y') = -\delta(\tau - \tau')\delta(x - x')\delta(y - y') \ . \tag{3.19}$$

Eq. (3.15) is a remarkable result. In the $N_f \to 0$ quenched approximation the full fermion Green's function still consists of a complicated set of Feynman diagrams that are normally not resummable. In particular at the two-loop level there are rainbow diagrams (Fig. 3.2(c)) and vertex-corrections of self-energies (Fig. 3.2(b)) that do not readily combine to a summable series. The reason why in this $N_f \to 0$ planar patch theory

we can do so, is the existence of the following multiplicative identity of fermion propagators in the planar limit where the dynamics is effectively 1+1 dimensional.

$$G_0(\tau_1, x_1)G_0(\tau_2, x_2) = G_0(\tau_1 + \tau_2, x_1 + x_2)\left(G_0(\tau_1, x_1) + G_0(\tau_2, x_2)\right) \tag{3.20}$$

This identity follows directly from trivial equality

$$(G_0(\tau_1, x_1))^{-1} + (G_0(\tau_2, x_2))^{-1} = (G_0(\tau_1 + \tau_2, x_1 + x_2))^{-1}, \tag{3.21}$$

and has many corollary multiplicative identities for products of $n > 2$ planar fermion propagators. The usual perturbative series and the exact result Eq. (3.15) may seem different but their equality can be proven to all orders. We do so in Appendix 3.A, thereby unambiguously establishing that this is the exact fermion two-point function in the planar theory in the quenched approximation.

3.3 The physics of the planar quenched quantum critical metal

We now show that this all order result for the fermion Green's function, albeit in the quenched $N_f \to 0$ approximation, describes very special physics. In this approximation the fermionic excitations constitute a continuous spectrum of excitations with power-law tails analogous to a critical theory; in particular, there are no distinct quasiparticle excitations. Importantly, in the low energy limit this continuous spectrum centers at three distinct momenta with different exponents for the power-law fall-off.

To exhibit this exotic physics from the exact $N_f \to 0$ Green's function (3.15), we substitute the explicit form of the boson and fermion Green's functions and Fourier transform the internal integrals. For the exponent $I(\tau, x; 0)$ we then have:

$$I(\tau, x; 0) = \frac{\lambda^2}{8\pi^3}\int \mathrm{d}\omega \mathrm{d}k_x \mathrm{d}k_y \frac{\cos(\omega\tau - k_x x) - 1}{(i\omega - vk_x)^2(\omega^2 + k_x^2 + k_y^2)} \tag{3.22}$$

This integral can be done analytically to obtain (for $v^2 \neq 1$)

$$I(\tau, x; 0) = \frac{\lambda^2}{8\pi(1-v^2)} \left[\frac{(\tau - ivx)}{\sqrt{1-v^2}} \log \left(\frac{\tau - ivx + \sqrt{(1-v^2)\,(\tau^2+x^2)}}{\tau - ivx - \sqrt{(1-v^2)\,(\tau^2+x^2)}} \right) \right.$$
$$\left. -2\sqrt{\tau^2+x^2} \right]; \tag{3.23}$$

for $v^2 = 1$ one obtains

$$I_{v^2=1}(\tau, x; 0) = \lambda^2 \frac{(\tau + i\,\mathrm{sgn}(v)x)^2}{12\pi\sqrt{\tau^2+x^2}}. \tag{3.24}$$

This gives us the all order $N_f \to 0$ Green's function in real space.

Analytically continuing in τ for $0 < v < 1$ yields the retarded Green's function. The physics follows from Fourier transforming this real time Green's function to momentum space; this is described in Appendix 3.C. The resulting retarded Green's function in momentum space is given by

$$G_R(\omega, k_x) = \frac{1}{\omega - k_x v + \frac{\lambda^2}{4\pi\sqrt{1-v^2}}\sigma(\omega, k_x)}, \tag{3.25}$$

where $\sigma(\omega, k_x)$ is the root, within $0 < \mathrm{Im}(\sigma) < i\pi$, of the equation

$$\frac{\lambda^2}{4\pi\sqrt{1-v^2}}(\sinh(\sigma) - \sigma\cosh(\sigma)) + v\omega - k_x - \cosh(\sigma)(\omega - k_x v + i\epsilon) = 0 \tag{3.26}$$

A small positive parameter ϵ is introduced to identify the correct root when it otherwise would be on the real axis, which is the case for

$$(k_x + \omega)\left(\lambda^2 \sinh\left(\frac{4\pi\sqrt{1-v^2}(vk_x - \omega)}{\lambda^2}\right) + 4\pi\sqrt{1-v^2}(v\omega - k_x)\right) \geq 0. \tag{3.27}$$

Note that the center-combination $v\omega - k_x$ is correct; we are working in units in which the boson-dispersion velocity $c = 1$. The units can be made correct by restoring c.

Expression (4.4) together with (3.26) is the main technical result of the chapter. We can now extract the insights into the spectrum of fermionic

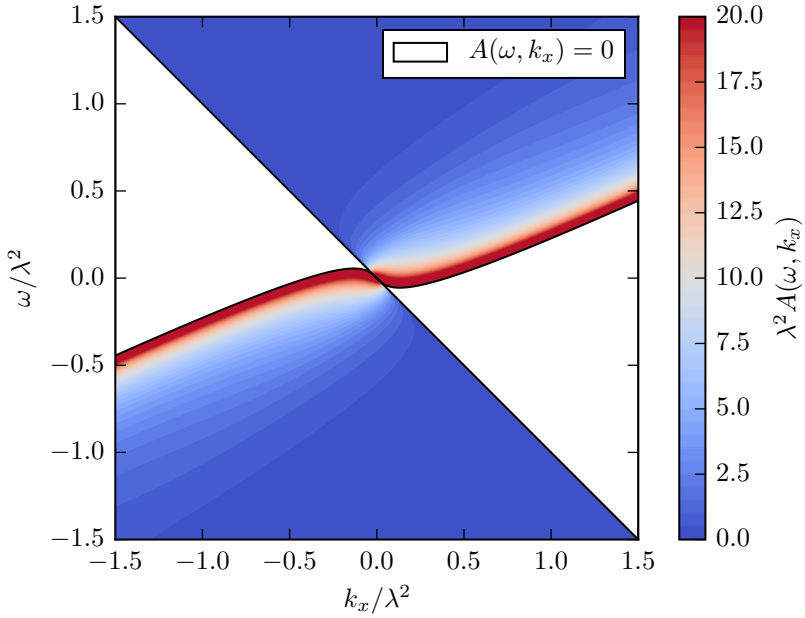

Figure 3.5. Fermionic spectral function for $v = 0.5$. It is identically zero in the white region.

excitations around the ground state of the planar quenched metal. Fig. 3.5 plots the spectral function $A(\omega, k_x) = -2\text{Im}G_R(\omega, k_x)$ as a function of the dimensionless combinations ω/λ^2, k_x/λ^2, as λ is the only scale in the problem. We immediately note that there is an obvious continuous peak, corresponding to a clear excitation in the spectrum. This excitation has the properties that:

- The dispersion relation is S-shaped in the infrared near $k_x = 0$, and now has three intersections with $\omega = 0$. A truncation of the theory to very low energies would therefore indicate three distinct Fermi surfaces. Similar topological Fermi surface instabilities due to electron interaction have been found e.g. in [40]. Curiously the dispersion is nearly identical to the one-loop result.

- As has been demonstrated before by means of a perturbative renormalization group analysis [27], we see the speed of fermions v decreases as we go from high to low frequency/momentum. The dis-

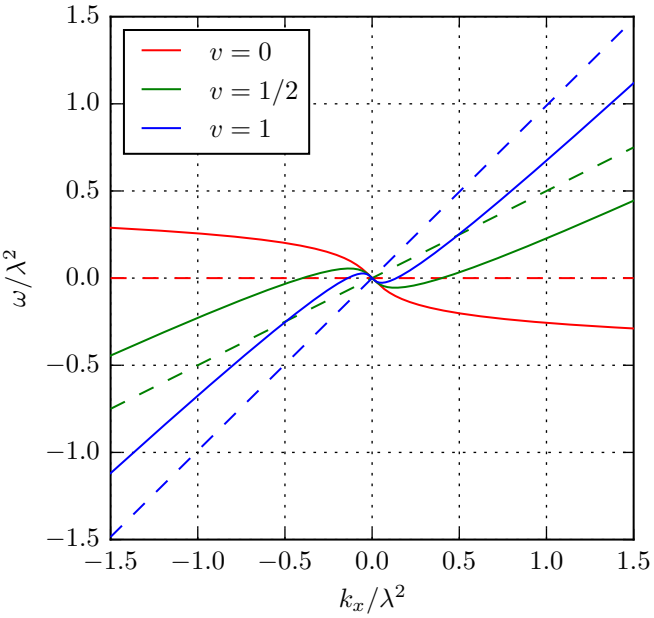

Figure 3.6. The dispersion relation (the zeros of G^{-1}) for different v in the interacting theory (solid line) and the free theory (dashed)

tinct S-shaped curve is outside of the regime of perturbation theory, however. With the exact result we see that the emergent Fermi-velocity at the innermost ($k_x = -k_x^* < 0$) and the outermost ($k_x = k_x^* > 0$) Fermi surfaces is non-universal, but positive and depends on the UV fermionic velocity v. These Fermi-surfaces are therefore particle-like.

However, the reverse of direction due to the S-shape shows that the Fermi velocity at the emergent Fermi-surface at the original Fermi-momentum $k_x = 0$ is now in the opposite direction and the surface is therefore hole-like. Moreover, the value of the emergent Fermi-velocity at $k_x = 0$ is universal: it equals the boson-velocity $v_F = -1$ at $k = 0$ (near the middle Fermi surface), independent of the UV fermionic velocity v (Fig. 3.6). A way to perceive what happens is that the hole-like excitations at $k_x = 0$ become tied to the critical boson which completely dominates the dynamics.

- The three emergent Fermi surfaces are symmetric around $k_x = 0$;

the hole-like one is at $k_x = 0$ and as follows from Eq. (4.4) and (3.26) the two particle-like ones are symmetrically arranged at $\pm k_x^*$. The precise value of k_x^* depends on the initial fermi velocity v. In the planar approximation where the Fermi surface is infinite in extent, this guarantees that Luttinger's theorem holds: the original Fermi surface (the region $-\infty < k_x < 0$) has the same volume as the emergent two regions enclosed by Fermi surfaces ($-\infty < k_x < -k_x^*$ and $0 < k_x < k_x^*$).

- The spectral function, $A(\omega, k_x) = -2\mathrm{Im}G_R(\omega, k_x)$, is identically zero for the range of ω and k_x whenever $\sigma(\omega, k_x)$ is exactly real. This is whenever Inequality (3.27) is satisfied. Such a large range of zero-weight may seem to violate unitarity. As a consistency check, however, it can be demonstrated that the Green's function satisfies the sum rule for all v (Appendix 3.D)

$$\int_{-\infty}^{\infty} \mathrm{d}\omega A(\omega, k_x) = 2\pi, \ \forall k_x \tag{3.28}$$

- Importantly, the weight of the spectral function is infinite at all points of the dispersion relation. Substituting the implicit dispersion relation $\sigma = \frac{4\pi\sqrt{1-v^2}}{\lambda^2}(\omega - vk_x)$ into the constraint Eq. (3.26), one can verify this explicitly. The spectrum is therefore a continuum, and not discrete. The excitation spectrum therefore resembles that of a scale-invariant critical theory, rather than that of interacting particles.

- Focusing on the low-energy regime, i.e. a narrow band in the spectral function around $\omega = 0$, we can determine the spectral weight analytically around the three different Fermi-surfaces — the three different crossings of the dispersion relation with $\omega = 0$. Expanding Eq. (3.26) around $(\omega, k_x) = (0, 0)$ the retarded Greens's function behaves as

$$G_R(\omega, k_x) = C\lambda^{-4/3} |\omega + k_x|^{-1/3}, \tag{3.29}$$

with $C = (1+v)^{1/3} \frac{4\pi}{(12\pi)^{1/3}} \left[i\frac{\sqrt{3}}{2} - \frac{1}{2}\,\mathrm{sgn}(\omega + k) \right]$, whereas near the outer Fermi surfaces $(\omega, k_x) = (0, \pm k_x^*)$ we have

$$G_R(\omega, k_x) \sim \lambda^{-1} (v^* k_x - \omega)^{-1/2}. \tag{3.30}$$

In each case the IR $\omega \simeq 0$ spectral function thus has a clear power-law behavior with a branch-cut singularity, but it has a different exponent depending on the Fermi surface. Furthermore, at the $k_x = 0$ Fermi surface the spectral function is symmetric around ω, while in the other two it is zero for negative (positive) frequencies. This is clearly visible in Fig. 3.5.

Interestingly, in all three cases the power-law scaling conforms with a uniform scaling of energy and momentum corresponding to ground-state with a dynamical critical exponent $z_f = 1$ (consistent with [26, 29]). This is in contrast to the expectation that the 2+1 dimensional quantum critical metal has a $z_f \neq 1$ groundstate [11]. However, the role of Landau damping and Fermi surface curvature is crucial in this expectation, and both are ignored in the planar $N_f = 0$ approximation here.

All these insights are non-perturbative. This can be readily shown by comparing our exact result to the one-loop perturbative answer (Fig. 3.7 and Fig. 3.8). The one-loop result is only a good approximation in the UV, far away from the continuous set of excitations, i.e. the dimensionful Yukawa coupling $\lambda^2 \ll |\omega - v k_x|$. Perturbation theory therefore fails to capture any of the distinct non-Fermi liquid phenomenology of IR of the planar quenched model (with the exception of the shape of the dispersion-curve). Despite the fact that this is not the true IR of the full theory, where Landau damping must also be taken into account, for energies and temperatures slightly above E_{LD} the full physics will resemble this quenched critical non-Fermi-liquid result.

For completeness we can also compute the density of states and the occupation number as a function of momentum. The former gives (see Appendix 3.D)

$$N(\omega) = \int \mathrm{d}k_x \frac{A(\omega, k_x)}{2\pi} = \frac{1}{v}\left[1 + \theta(\lambda^2 \frac{\cosh^{-1}(v^{-1}) - \sqrt{1-v^2}}{4\pi(1-v^2)^{3/2}} - |\omega|)\right]. \tag{3.31}$$

The occupation number can be obtained from the spectral function by using the formula

$$n_{k_x} = \int_{-\infty}^{0} \mathrm{d}\omega \frac{A(\omega, k_x)}{2\pi} \tag{3.32}$$

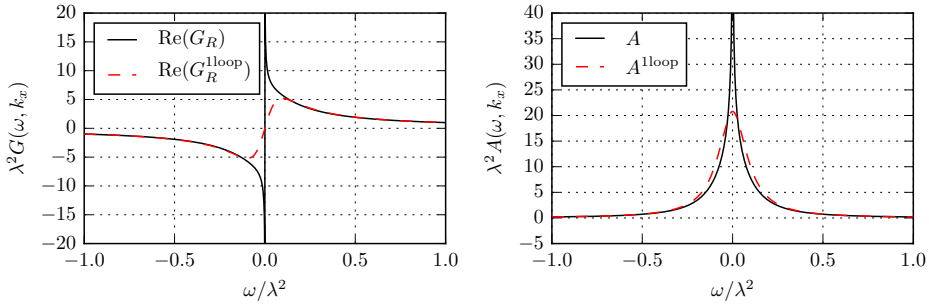

Figure 3.7. The real and the imaginary part of the Green's function at the middle Fermi surface ($k_x = 0$, $v = 0.5$) as a function of ω (solid line), compared with the corresponding one-loop result (dashed)

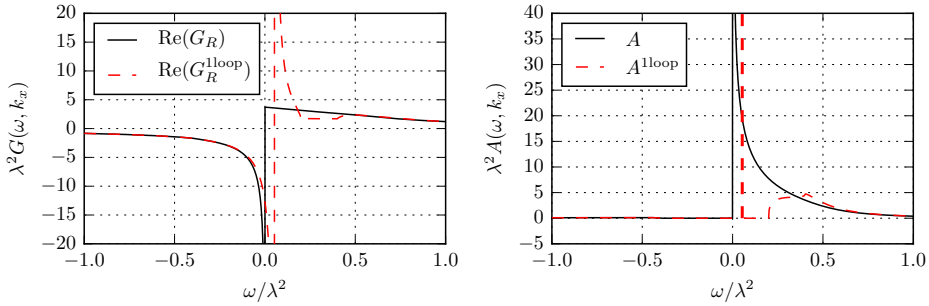

Figure 3.8. The real and the imaginary part Green's function at the outer Fermi surface ($k_x = k_x^* \approx 0.4\lambda^2$, $v = 0.5$) as a function of ω (solid line), and the one-loop truncated result (dashed). The spectral weight of the one-loop approximation is concentrated to a δ-function whereas the spectral weight of the full result is spread in the power-law singularity.

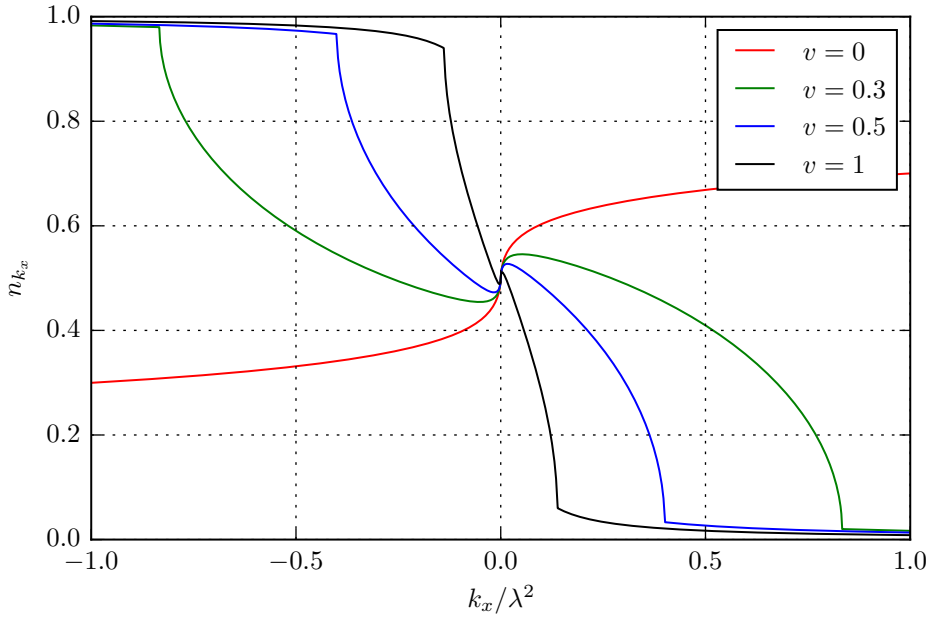

Figure 3.9. The occupation number for different v as a function of momentum. We can see the effect of the multiple sharp fermi surfaces, the non-fermi liquid behaviour is also apparent as a non-monotonic behaviour of the occupation number.

This evaluates to (Appendix 3.D)

$$n_{k_x} = \frac{1}{\pi} \arg \left[\frac{\cosh(\sigma(\omega = 0, k_x/\lambda^2, v)) - v}{v \cosh^{-1}(v) - \sqrt{1 - v^2}(i - 4\pi(1 - v^2)k_x/\lambda^2)} \right], \qquad (3.33)$$

where $\sigma(\omega, k_x)$ is defined by (3.26). It is plotted in Fig. 3.9. We can see the effect of the multiple Fermi surfaces as discontinuities in the derivative of the occupation number, even though the occupation number itself is continuous. This is another way to see that the fermionic excitation spectrum is that of a non-Fermi liquid. (Note that in the singular case of vanishing UV Fermi velocity $v = 0$, the occupation number has different asymptotics as $k_x \to \pm\infty$ than for any small but non-zero v. For $v \neq 0$ the occupation number approaches $n_{k_x} = 1$ at $k_x = -\infty$ and $n_{k_x} = 0$ at $k_x = \infty$, as it should.)

3.4 Conclusions

In this chapter we have shown that in the quenched $N_f \to 0$ limit the fermion Green's function in a 2+1 dimensional quantum critical metal can be determined exactly. The quenched limit neuters the dangerous nature of dimensionally irrelevant Fermi surface corrections and allows us to truncate to a linear dispersion relation for the fermions. This reduction to an effective one-dimensional system allows an explicit solution to the fermion Green's function in the presence of a background scalar field. The quenched $N_f \to 0$ limit further allows us to compute the full background scalar field path-integral when coupled minimally to the fermion.

Even though the quenched limit discards the physics of Landau damping, our result shows that the resulting physics is already very non-trivial. There are three distinct low-energy excitations as opposed to the excitations around a single Fermi surface of the free theory. Most importantly, the sharp excitations of the free theory broaden into a power-law singularity of the spectral function of the form $G \sim (\omega - \epsilon(k_x))^{-\eta}$, with either $\eta = 1/2$ or $\eta = 1/3$. The groundstate is a non-Fermi-liquid.

Beyond the quenched limit and including N_f corrections, i.e. fermion loops, Landau damping effects become important. These effects will show up below some energy scale E_{LD} set by both N_f and the Fermi surface curvature κ. Our model breaks down below this scale, but it is expected to describe the physics above E_{LD}. What our results show is that, qualitatively, the physics is that of a non-Fermi-liquid both above E_{LD} and below E_{LD} [38], but in detail it will differ.

In order to access IR physics below E_{LD}, the corrections in the Fermi surface curvature and the number of fermionic flavours must be treated systematically, but a (possible) shortcut deserves to be mentioned. Our analytic determination of the exact fermionic Green's analytically hinged on the free fermion dispersion being linear, but the approach taken in this chapter does not put any restrictions on the allowed form of the bosonic propagator. This opens up the possibility to implement the Landau-damping effects phenomenologically, just by modifying the background bosonic Green's function, and staying within the Gaussian approximation. This is the approach taken by Khveshchenko and Stamp [36] and Altshuler, Lidsky, Ioffe and Millis [37, 38]. Comparing to vector large N_f approaches [20, 21], it is not clear that this is sufficient to reliably capture the IR. The Landau damping is not the only important effect. Interactions of the boson field with itself beyond the Gaussian approximation

must also be taken into account, e.g. our model needs to be enhanced by a ϕ^4 interaction to describe the Ising-nematic critical point [39].

The interesting question will be which non-Fermi liquid features are retained and which change. The dynamical critical exponent z_f below the Landau damping scale is likely different from 1. Also, the splitting of the Fermi surface seems to be a subtle phenomenon, and whether it remains stable upon including fermionic loop corrections or going beyond the local patch approximation requires a careful investigation. On the other hand, the destruction of the quasi-particle poles and the fact that the spectrum is singular along the full dispersion curve is expected to be a robust effect that resembles that of a critical state. This is thought to be enhanced by the Landau damping.

3.A Comparison with perturbation theory

We can expand (3.15) in the coupling constant. Although at first sight this expansion seems different from the usual perturbative expansion, we will show that in the case of zero fermi surface curvature they match at any order if we do not include fermion loops.

The λ^{2n} term in (3.15) is

$$G_n(z) = \frac{G_0(z)}{2^n n!}\Big(\int dx' dx'' d\tau' d\tau'' \left[G_0\left(z-z'\right)+G_0\left(z'\right)\right] G_B\left(z'-z''\right) \left[G_0\left(z-z''\right)+G_0\left(z''\right)\right] \Big)^n, \tag{3.34}$$

where $z = x + iv\tau$. The usual perturbative expansion result can be obtained by expanding

$$\langle \psi(z)\psi(0)^\dagger \exp(\lambda\phi\psi^\dagger\psi)\rangle \tag{3.35}$$

and evaluating by Wick contraction

$$G_n^{\text{pert}}(z) = \frac{(2n-1)!!}{(2n)!}\int dx_1 ... dx_{2n} d\tau_1 ... d\tau_{2n} I \cdot G_B(x_1-x_2,\tau_1-\tau_2)...\cdot \cdot G_B(x_{2n-1}-x_{2n},\tau_{2n-1}-\tau_{2n}), \tag{3.36}$$

$$I = \sum_{(i_1,..,i_{2n})\in S_{2n}} G_0\left(z - z_{i_1}\right) G_0\left(z_{i_1} - z_{i_2}\right) ... G_0\left(z_{i_{2n-1}} - z_{i_{2n}}\right) G_0\left(z_{i_{2n}}\right) \tag{3.37}$$

Here S_n is the set of permutations of the numbers 1 through n. The factor $1/(2n!)$ comes from the Taylor expansion of the exponential. By summing over the different assignments of internal points we are explicitly counting the different contractions of the fermion fields. There are however still $(2n-1)!!$ possibilities to pair the boson fields (each pairing gives rise to the same contribution after a change of variable in the integral). Since $(2n)!/(2n-1)!! = n! \cdot 2^n$ the identity which remains to be proved, once we have used our simple form of the free fermion Green's function, is

$$\sum_{(i_1,..,i_m)\in S_m} \frac{1}{z - z_{i_1}} \frac{1}{z_{i_1} - z_{i_2}} ... \frac{1}{z_{i_{m-1}} - z_{i_m}} \frac{1}{z_{i_m}} = \tag{3.38}$$

$$= \frac{z^{m-1}}{\left(z - z_1\right)\left(z - z_2\right) ... \left(z - z_m\right) z_1 ... z_m}. \tag{3.39}$$

We need this for $m = 2n$, but the statement is true for odd m as well.

The identity can be proven by induction. The $m = 1$ case is easily checked and given that the equality holds for $m - 1$ we have

$$\sum_{(i_1,..,i_m)\in S_m} \frac{1}{z - z_{i_1}} \frac{1}{z_{i_1} - z_{i_2}} ... \frac{1}{z_{i_{m-1}} - z_{i_m}} \frac{1}{z_{i_m}} = \tag{3.40}$$

$$= \frac{1}{z_1 ... z_m} \sum_{k=1}^{m} \frac{1}{z - z_k} \frac{z_k^{m-1}}{\left(z_k - z_1\right)\left(z_k - z_2\right) ... \left(z_k - z_m\right)}.$$

where the product in the last denominator excludes $(z_k - z_k)$. The right hand side of (3.39) and (3.40) are the same since they are both meromorphic functions of z with the same pole locations and residues and they both approach 0 at ∞.

3.B Calculating the real-space fermion Green's function

To find the real-space Euclidean fermionic Green's function we have to evaluate the integral (3.22). In order to do that, it is convenient to firstly

make a coordinate transformation of the following form

$$\begin{aligned}\omega &= \frac{xk_1 + \tau k_2}{\sqrt{x^2+\tau^2}},\\ k_x &= \frac{xk_1 - \tau k_2}{\sqrt{x^2+\tau^2}}.\end{aligned} \tag{3.41}$$

The integral in k_2 can be then explicitly evaluated, giving

$$\int \mathrm{d}k_1 \mathrm{d}k_y \frac{\lambda^2\left(\tau^2+x^2\right)\left(\cos\left(k_1\sqrt{\tau^2+x^2}\right)-1\right)}{8\pi^2\sqrt{k_1^2+k_y^2}\left(x\left(\sqrt{k_1^2+k_y^2}+|k_1|v\right)-i\tau\left(v\sqrt{k_1^2+k_y^2}+|k_1|\right)\right)^2}. \tag{3.42}$$

Now switching to polar coordinates, $k_1 = k\cos\theta$, $k_y = k\sin\theta$, and performing the radial integral in k we obtain

$$I = \int_0^{2\pi} \mathrm{d}\theta \frac{\lambda^2|\sin(\theta)|\left(\tau^2+x^2\right)^{3/2}}{16\pi(\tau v + ix + |\sin(\theta)|(ivx+\tau))^2}. \tag{3.43}$$

Finally, integrating over θ for $v^2 \neq 1$ we derive

$$I = \frac{\lambda^2}{8\pi(1-v^2)}\left(\frac{(\tau+ivx)}{\sqrt{1-v^2}}\log\left(\frac{\tau+ivx+\sqrt{(1-v^2)\left(\tau^2+x^2\right)}}{\tau+ivx-\sqrt{(1-v^2)\left(\tau^2+x^2\right)}}\right) - 2\sqrt{\tau^2+x^2}\right). \tag{3.44}$$

For the specific case $v^2 = 1$ the integration should be done independently and gives a simpler result

$$I = \lambda^2\frac{(\tau - i\,\mathrm{sgn}(v)x)^2}{12\pi\sqrt{\tau^2+x^2}}. \tag{3.45}$$

To Fourier transform the corresponding Green's function to momentum space, we will need an analytical continuation. For $0 < v < 1$, (3.15) with exponent (3.44) can be analytically continued in τ to the complex plane with two branch-cuts along parts of the imaginary axis

$$G_E(x,\tau) = -\frac{i}{2\pi}\frac{\mathrm{sgn}(v)}{x+iv\tau}\cdot \\ \cdot e^{\frac{\lambda^2}{8\pi(1-v^2)}\left(\frac{(\tau+ivx)}{\sqrt{1-v^2}}\left(i\pi\mathrm{sgn}(x)+2\tanh^{-1}\left(\frac{\tau+ivx}{\sqrt{(1-v^2)(\tau^2+x^2)}}\right)\right)-2\sqrt{\tau^2+x^2}\right)} \tag{3.46}$$

3.C Fourier transforming the fermion Green's function

The next step is to calculate the retarded fermionic Green's function in momentum space. We know that the time-ordered momentum space Green's function of the Lorentzian signature theory, $G_T(\omega)$, is related to the Green's function of the Euclidean theory, $G_E(\omega)$, by analytical continuation

$$G_T(\omega, k_x) = G_E(\omega(-i+\epsilon), k_x). \tag{3.47}$$

$G_T(\omega, k_x)$ is analytic below the real line in the left half plane and above the real line in the right half plane. $G_E(\omega, k_x)$ is the Fourier transform in a generalized sense of (3.46). The (rather severe) divergence at infinity has to be regularized. Since the expression we found in Appendix 3.B permitted an analytic continuation to all of the first and third quadrants, we can continuously rotate the integration contour in the Fourier transform, $\tau = t(i+\delta)$, if additionally there is a regulator analytic in the first and third quadrant. We thus have

$$G_T(\omega, k_x) = \int \mathrm{d}t(i+\delta)\mathrm{d}x \mathrm{e}^{i(\omega(-i+\epsilon)(i+\delta)t - k_x x)} G_E(t(i+\delta), x). \tag{3.48}$$

From this we see that the real-space time-ordered Green's function is given by analytically continuing the real-space Green's function of the Euclidean theory

$$G_T(t, x) = iG_E(t(i+\delta), x). \tag{3.49}$$

This slightly heuristic argument of analytical continuation in real space has been verified to give the correct Green's function up to one loop perturbation theory. The retarded Green's function is given by

$$G_R(\omega, k_x) = \int \mathrm{d}t\mathrm{d}x \mathrm{e}^{i(\omega t - k_x x)} \theta(t)(G_T(t, x) + G_T^*(-t, -x)). \tag{3.50}$$

$G_T(t, x)$ is of the form $t^{-1} f_1(x/t) \exp(\lambda^2 t f_2(x/t))$. By performing a change of variable from x to $u = x/t$ we can perform the t integral. For this we need a regulator $\exp(-\epsilon t)$. The integrand of the remaining u integral has compact support, $u \in [-1, 1]$. We can perform a further change of variables

$$\sigma = \tanh^{-1}\left(\frac{\sqrt{(1-v^2)(1-u^2)}}{1-uv}\right). \tag{3.51}$$

This function maps $[-1, v) \to \mathbb{R}^+$ and $(v, 1] \to \mathbb{R}^+$, both bijectively. The inverse thus has two branches that we need to integrate over, one for $u < v$ and one for $u > v$, and both integrals will be over $\mathbb{R}^+$. This change of variable is consistent with the principal value integral required for the singularity at $u = v$ if the $\sigma \to \infty$ limits are performed at the same time. The integrand obtained with this change of variable can be written as a sum of four pieces

$$G_R(\omega, k_x) = \int_0^\infty \mathrm{d}\sigma \Big[F(\sigma) + F(-\sigma) - F(\sigma + i\pi) - F(-\sigma + i\pi) \Big], \quad (3.52)$$

where $F(\sigma)$ is defined as

$$F(\sigma) = \frac{i}{2\pi} \frac{\sinh(\sigma)}{\frac{\lambda^2(\sinh(\sigma) - \sigma\cosh(\sigma))}{4\pi\sqrt{1-v^2}} + v\omega - k_x - \cosh(\sigma)(\omega - k_x v + i\epsilon)}. \quad (3.53)$$

Since $F(\sigma)$ is a meromorphic function and it approaches 0 as $\mathrm{Re}(\sigma) \to \pm\infty$, we can close the contour at $\pm\infty$ and obtain the integral as the residue of $F(\sigma)$'s single pole in the strip $0 < \mathrm{Im}(\sigma) < i\pi$,

$$G_R(\omega, k_x) = \frac{1}{\omega - k_x v + \frac{\lambda^2}{4\pi\sqrt{1-v^2}}\sigma(\omega, k_x)} \quad (3.54)$$

where $\sigma(\omega, k_x)$ is the solution, within $0 < \mathrm{Im}(\sigma) < i\pi$, of the equation

$$0 = \frac{\lambda^2}{4\pi\sqrt{1-v^2}}(\sinh(\sigma) - \sigma\cosh(\sigma)) + v\omega - k_x - \cosh(\sigma)(\omega - vk_x + i\epsilon). \quad (3.55)$$

The dispersion, $\omega(k_x)$, given by the location of the singularity of $G(\omega, k_x)$ is no longer monotonic as in the free case. The singularity occurs when the roots of (3.55) leave the real line. The dispersion can not be found analytically in general but for the two points where $\mathrm{d}\omega/\mathrm{d}k_x = 0$ we have,

$$\begin{aligned} \omega &= \pm\lambda^2 \frac{\sqrt{1-v^2} - \cosh^{-1}(v^{-1})}{4\pi(1-v^2)^{3/2}}, \\ k_x &= \pm\lambda^2 \frac{\sqrt{1-v^2} - v^2\cosh^{-1}(v^{-1})}{4\pi v(1-v^2)^{3/2}}. \end{aligned} \quad (3.56)$$

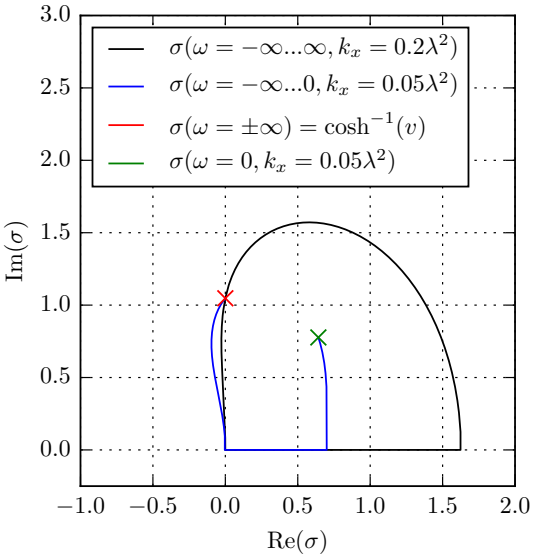

Figure 3.10. This figure shows a closed contour of integration for the sum rule and an open contour for calculating the occupation number integral. $v = .5$.

3.D Integrals of the spectral function

Several important observables like the density of states or the occupation number are defined by momentum space integrals of the spectral function $A(\omega, k) = -2\text{Im}G_R(\omega, k)$. Despite the fact that we have only an implicit expression for the Green's function (3.54), these integrals can be relatively easily evaluated by bringing the imaginary axis projection outside the integral and then changing integration variable to σ. We then do not have a closed form expression for the (now complex) contour of integration but the integrand is greatly simplified.

For a fixed k_x we have ω as a closed form function of σ. Making this change of variable in integrals over ω gives the integrand

$$\int_C \mathrm{d}\omega A(\omega, k_x) = -2\text{Im}\left(\int_{\sigma(C)} \mathrm{d}\sigma \frac{\sinh(\sigma)}{v - \cosh(\sigma)}\right). \tag{3.57}$$

The curve of integration, $\sigma(C)$, is now defined through the implicit expression for σ in (3.55).

First of all we check that the sum rule $\int \mathrm{d}\omega A(\omega, k_x) = 2\pi$ is satisfied. Taking the $\omega \to \pm\infty$ limits in (3.55) we see that σ approaches $\cosh^{-1}(v)$ in both limits and the curve is thus closed. See Fig. 3.10. To solve the integral we thus just have to figure out what poles are within the contour. It turns out that the single pole is the one at $\sigma = \cosh^{-1}(v)$, which is on the contour. This gives divergences but since the residue is real they are in the real part and do not matter for the spectral density. The contribution to the imaginary part is just $2\pi i$ times half the residue since the contour is smooth at the pole. The result of the integral is then 2π as expected, for all values of k_x/λ^2 and v.

The occupation number at zero temperature is given by

$$\rho(k_x) = \int_{-\infty}^{0} \frac{\mathrm{d}\omega}{2\pi} A(\omega, k_x). \tag{3.58}$$

Since this contour is not closed we find a primitive function defined along the whole contour. The contribution from the point $\omega = 0$ depends on $\sigma(\omega = 0, k_x, v)$ so we can not get a closed form expression in this case. The contribution from $\omega \to -\infty$ now depends on the direction of the limit in the complex σ-plane since the point is only approached from one side. Summing the contributions from the two endpoints of the integral gives

$$\rho(k_x) = \frac{1}{\pi} \arg\left[\frac{\cosh(\sigma(\omega = 0, k_x/\lambda^2, v)) - v}{v\cosh^{-1}(v) - \sqrt{1-v^2}(i - 4\pi(1-v^2)k_x/\lambda^2)} \right]. \tag{3.59}$$

From this we see that in the region where σ is real we actually have a closed form expression for the occupation number.

The density of states, $N(\omega) = \int \mathrm{d}k_x A(\omega, k_x)$ is similarly calculated by changing variables to σ. For any ω there is a K_x such that $\sigma(k_x)$ is real for all $|k_x| > K_x$. The limits $k_x \to \pm\infty$ give $\sigma \to \pm\cosh^{-1}(1/v)$ and these are thus approached along the real line. Once again the integrand has poles (residue 1/v) at these points and since we are only interested in the imaginary part of the integral of the retarded Green's function we will only need to know the direction we approach these poles from. Finding a primitive function is again trivial and in the end the result only depends on the direction the poles are approached from. Since σ is real in the limits, each pole is approached from either the left or the right. There are three different cases, for

$$\omega < -\lambda^2 \frac{\cosh^{-1}\left(v^{-1}\right) - \sqrt{1-v^2}}{4\pi(1-v^2)^{3/2}} \tag{3.60}$$

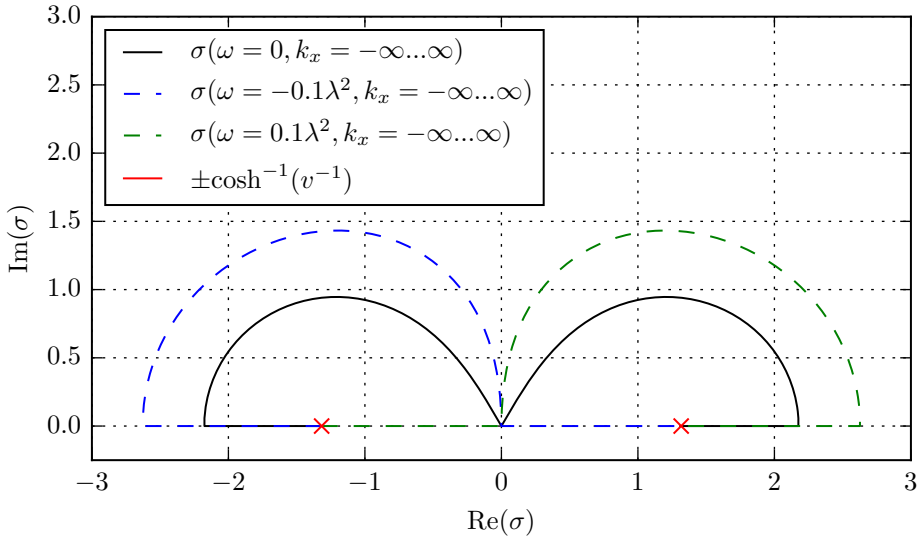

Figure 3.11. Integration contours for calculating density of states. The integrand and locations of the endpoints are independent of ω but since the integrand has poles at the endpoints the direction of approach matters. The poles are always approached along the real axis and this figure shows the three possible configurations. $v = .5$.

both poles are approached from the left. For

$$\omega > \lambda^2 \frac{\cosh^{-1}\left(v^{-1}\right) - \sqrt{1-v^2}}{4\pi(1-v^2)^{3/2}} \tag{3.61}$$

both poles are approached from the right and for ω between these two values the left pole is approached from the left and the right pole from the right. See Fig. 3.11. Taking these different limits of the primitive function gives

$$N(\omega) = \frac{1}{v}\left[1 + \theta(\lambda^2 \frac{\cosh^{-1}\left(v^{-1}\right) - \sqrt{1-v^2}}{4\pi(1-v^2)^{3/2}} - |\omega|)\right]. \tag{3.62}$$

The density of state takes two different values and we see that the ω where it changes are exactly the points where there are two instead of one solution in k_x to the equation $G^{-1}(\omega, k_x) = 0$.

Bibliography

[1] L. D. Landau, "The theory of a Fermi liquid," Sov. Phys. Jetp-Ussr **3(6)**, 920-925 (1957)

[2] C. M. Varma, P. B. Littlewood, S. Schmitt-Rink, E. Abrahams and A. E. Ruckenstein, "Phenomenology of the normal state of Cu-O high-temperature superconductors," Phys. Rev. Lett. **63** (1989) 1996

[3] Y. Barlas and K. Yang, "Non-Fermi-liquid behavior in neutral bilayer graphene," Phys. Rev. B **80** (2009) 161408(R); arXiv:0908.1238 [cond-mat.mes-hall]

[4] F. Guinea and M. I. Katsnelson, "Many-Body Renormalization of the Minimal Conductivity in Graphene," Phys. Rev. Lett. **112** (2014) 116604; arXiv:1307.6221 [cond-mat.mes-hall]

[5] D. van der Marel, H. J. A. Molegraaf, J. Zaanen, Z. Nussinov, F. Carbone1, A. Damascelli, H. Eisaki, M. Greven, P. H. Kes, M. Li "Quantum critical behaviour in a high-Tc superconductor," Nature 425, 271-274 (2003); arXiv:cond-mat/0309172

[6] P. Gegenwart, Q. Si, F. Steglich, "Quantum criticality in heavy-fermion metals," Nature Physics 4, 186 - 197 (2008); arXiv:0712.2045 [cond-mat.str-el]

[7] T. Senthil, "Theory of a continuous Mott transition in two dimensions," Phys. Rev. B **78** (2008) 045109; arXiv:0804.1555 [cond-mat.str-el]

[8] T. Misawa and M. Imada, "Quantum criticality around metal–insulator transitions of strongly correlated electron systems," Phys. Rev. B **75** (2007) 115121; arXiv:cond-mat/0612632

[9] J. A. Hertz, "Quantum critical phenomena," Phys. Rev. B **14** (1976) 1165

[10] A. .J. Millis, "Effect of a nonzero temperature on quantum critical points in itinerant fermion systems", Phys. Rev. B **48**, 7183 (1993).

[11] S. Sachdev, "Quantum phase transitions," 2nd Edition, Cambridge University Press 2011 (Chapter 18 especially).

[12] J. Rech, C. Pepin, A. V. Chubukov, "Quantum critical behavior in itinerant electron systems: Eliashberg theory and instability of a ferromagnetic quantum critical point," Phys. Rev. B, f74(19) (2006) 195126; arXiv:cond-mat/0605306

[13] S. Chakravarty, B. I. Halperin and D. R. Nelson, "Two-dimensional quantum Heisenberg antiferromagnet at low temperatures," Phys. Rev. B **39** (1989) 2344

[14] Q. Si, J. L. Smith, K. Ingersent, "Quantum critical behavior in Kondo systems," Int. J. Mod. Phys. B **13** (1999) 2331; arXiv:cond-mat/9905006

[15] H. v. Löhneysen, A. Rosch, M. Vojta, P. Wölfle, "Fermi-liquid instabilities at magnetic quantum phase transitions" Rev. Mod. Phys. **79**, 1015 (2007).

[16] M. A. Metlitski and S. Sachdev, "Quantum phase transitions of metals in two spatial dimensions: I. Ising-nematic order," Phys. Rev. B **82** (2010) 075127 arXiv:1001.1153 [cond-mat.str-el]

[17] M. A. Metlitski and S. Sachdev, "Quantum phase transitions of metals in two spatial dimensions: II. Spin density wave order," Phys. Rev. B **82** (2010) 075128 arXiv:1005.1288 [cond-mat.str-el]

[18] T. Holder and W. Metzner, "Anomalous dynamical scaling from nematic and U(1)-gauge field fluctuations in two dimensional metals," Phys. Rev. B **92** (2015) 4, 041112 arXiv:1503.05089 [cond-mat.str-el]

[19] T. Holder and W. Metzner, "Fermion loops and improved power-counting in two-dimensional critical metals with singular forward scattering," arXiv:1509.07783 [cond-mat.str-el]

[20] S. S. Lee, "Low-energy effective theory of Fermi surface coupled with U(1) gauge field in 2+1 dimensions," Phys. Rev. B **80** (2009) 165102; arXiv:0905.4532 [cond-mat.str-el]

[21] D. F. Mross, J. McGreevy, H. Liu and T. Senthil, "A controlled expansion for certain non-Fermi liquid metals," Phys. Rev. B **82** (2010) 045121; arXiv:1003.0894 [cond-mat.str-el]

[22] A. L. Fitzpatrick, S. Kachru, J. Kaplan and S. Raghu, "Non-Fermi liquid fixed point in a Wilsonian theory of quantum critical metals," Phys. Rev. B **88** (2013) 125116 arXiv:1307.0004 [cond-mat.str-el]

[23] A. L. Fitzpatrick, S. Kachru, J. Kaplan and S. Raghu, "Non-Fermi-liquid behavior of large-N_B quantum critical metals," Phys. Rev. B **89** (2014) 16, 165114 arXiv:1312.3321 [cond-mat.str-el]

[24] R. Mahajan, D. M. Ramirez, S. Kachru and S. Raghu, "Quantum critical metals in $d = 3 + 1$ dimensions," Phys. Rev. B **88** (2013) 11, 115116 arXiv:1303.1587 [cond-mat.str-el]

[25] G. Torroba and H. Wang, "Quantum critical metals in $4 - \epsilon$ dimensions," Phys. Rev. B **90** (2014) 16, 165144 arXiv:1406.3029 [cond-mat.str-el]

[26] J. P. Blaizot and E. Iancu, "The Bloch-Nordsieck propagator at finite temperature," Phys. Rev. D **56** (1997) 7877 arXiv:hep-ph/9706397

[27] M. F. L. Golterman, "Chiral perturbation theory and the quenched approximation of QCD," Acta Phys. Polon. B **25**, 1731 (1994) arXiv:hep-lat/9411005

[28] A. Jakovac and P. Mati, "Resummations in the Bloch-Nordsieck model," Phys. Rev. D **85** (2012) 085006 arXiv:1112.3476 [hep-ph]

[29] A. Kernemann and N. G. Stefanis, "Exact Solutions for Fermionic Green's Functions in the Bloch-nordsieck Approximation of QED," Phys. Rev. D **40** (1989) 2103

[30] A. Jakovác and P. Mati, "Spectral function of the Bloch-Nordsieck model at finite temperature," Phys. Rev. D **87** (2013) 12, 125007 arXiv:1301.1803 [hep-th]

[31] A. Jakovác and P. Mati, "Validating the 2PI resummation: the Bloch-Nordsieck example," Phys. Rev. D **90** (2014) 4, 045038 arXiv:1405.6576 [hep-th]

[32] A. I. Karanikas, C. N. Ktorides and N. G. Stefanis, "On the infrared structure of the one fermion Green's function in QED," Phys. Lett. B **289** (1992) 176

[33] D. V. Khveshchenko and P. C. E. Stamp, "Low-energy properties of two-dimensional fermions with long-range current-current interactions", Phys. Rev. Lett. **71** (1993) 2118

[34] L. B. Ioffe, D. Lidsky, B. L. Altshuler, "Effective lowering of the dimensionality in strongly correlated two dimensional electron gas", arXiv:cond-mat/9403023.

[35] B. L. Altshuler, L. B. Ioffe, A. J. Millis, "On the low energy properies of fermions with singular interactions", Phys. Rev. **B50**, 14048. arXiv:cond-mat/9406024.

[36] A. Allais and S. Sachdev, "Spectral function of a localized fermion coupled to the Wilson-Fisher conformal field theory," Phys. Rev. B **90** (2014) 3, 035131 arXiv:1406.3022 [cond-mat.str-el]

[37] J. Quintanilla and A. J. Schofield, "Pomeranchuk and topological Fermi surface instabilities from central interactions," Phys. Rev. B **74** (2006) 115126; arXiv:cond-mat/0601103 [cond-mat.str-el]

[38] A. Neumayr and W. U. Metzner, "Fermion loops, loop cancellation and density correlations in two-dimensional Fermi systems,' Phys. Rev. B **58** (1998) 15449 doi:10.1103/PhysRevB.58.15449 [cond-mat/9805207]